J. Mech. Phys. Solids Vol. 41, No. 7, pp. 1155–1176, 1993.
Printed in Great Britain.

0022–5096/93 $6.00 + 0.00
Pergamon Press Ltd

MODELS FOR BREAKDOWN-RESISTANT DIELECTRIC AND FERROELECTRIC CERAMICS

Z. SUO

Mechanical and Environmental Engineering Department, University of California, Santa Barbara, CA 93106-5070, U.S.A.

(*Received* 21 *September* 1992; *in revised form* 15 *February* 1993)

ABSTRACT

MODELS FOR dielectric breakdown are proposed and analysed, with emphasis on concepts leading to breakdown-resistant materials. The Griffith energy balance is extended to cracks under combined electrical and mechanical loading, and to conductive tubular channels. Breakdown strength for a perfect crystal is estimated by an analogue of the Frenkel model. In a crystal subjected to an electric field the equilibrium displacement of the electron clouds is described by a curve with periodicity of the lattice constant. A theory of breakdown-resistant laminates is proposed on the basis of charge relocation, facilitated by breakdown of the weak layers and the interfaces. A process by which a conducting path grows like a crack in ferroelectric ceramics is discussed, followed by an outline of fields around conducting cracks in piezoelectric ceramics.

1. INTRODUCTION

BREAKDOWN of solid dielectrics is a performance-limiting property in integrated circuits (DEVINE, 1988), as well as in power transmission cables (BRADWELL, 1983). The measured breakdown strength is sensitive to defects, electrodes (both material and geometry), and environment. A perspective on defect-tolerant, breakdown-resistant dielectrics is needed in an era in which complex materials can be tailored to meet specific needs.

When a dielectric is subjected to a low electric field, a small, uniformly distributed current density passes through the sample, as in a semiconductor. The dielectric breaks down when the current rises sharply at a critical electric field; permanent damage is often found along fine tubular channels, the major portion of the sample being left intact. A defect-free sample breaks down at a field specific to the material, invariant from sample to sample. This solid state phenomenon has been attributed to a few electrons in the conduction band, accelerated by the applied field, liberating more valance or trapped electrons. Models and experimental data of this type have been reviewed by WHITEHEAD (1953) and O'DWYER (1973).

Despite its fundamental significance, the intrinsic breakdown is rarely observed in practice. Inhomogeneities reduce the breakdown strength. For example, a perfect mica sample breaks down at a field above 1 GV m^{-1}, but samples of natural mica break down at fields as low as a few megavolts per meter with large statistical scatter.

Breakdown strengths of ceramics obey the Weibull statistics; the strengths measured with samples of similar size decrease as the grain size increases (FREIMAN and POHANKA, 1989). High field conduction and dielectric loss also affect breakdown strength.

Damage-localization and background dissipation prompt the analogy between dielectric breakdown and tensile fracture. Over the past half century, fracture mechanics has not only led to an understanding of conventional materials, but also inspired concepts of novel materials having unique property profiles. The basic ideas of fracture mechanics should be relevant to other localized damage phenomena, no matter whether they are activated by tensile stress or electric field.

In developing a perspective on breakdown, one would like to retain as many features of fracture mechanics as the subject would allow. Yet one faces immediate challenges. First, rather than crack-like growth, breakdown currents often create tubular channels. Second, the fundamental cause of breakdown usually has little to do with atomic debonding. Third, the dissipation mechanism accompanying breakdown is not plastic flow, but high field conduction. Building on two previous papers (SUO, 1991; SUO *et al.*, 1992), a new set of ideas is presented here to meet these challenges.

2. ENERGY BALANCE

A defect in a dielectric behaves either like a conductor or an insulator. Ionized gases, metallic precipitates and terminated electrodes are conductors. On the other hand, relative permittivities of ferroelectric ceramics exceed 10^3, so that gases inside a cavity, if not ionized, are insulators with much smaller permittivity. As illustrated in Fig. 1, an insulating crack intensifies the field applied perpendicular to the crack, but does not perturb the field parallel to the crack. Conversely, a conducting crack intensifies the field applied parallel to the crack, but not the field perpendicular to it. Also different is the sign of crack driving forces, being positive for a conducting crack and negative for an insulating crack. Consequently, under a monotonic field, an insulating crack will not grow but a conducting crack might. However, experiments by CAO and EVANS (1993) have shown that for ferroelectric ceramics under an

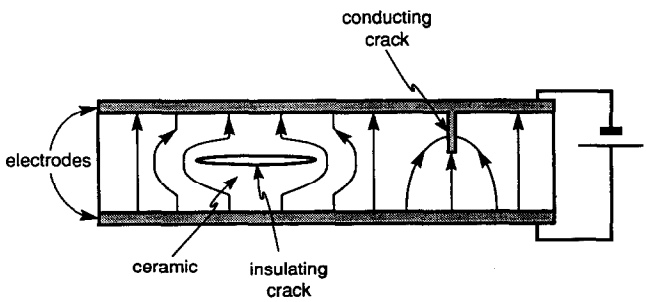

FIG. 1. An insulating crack intensifies the field applied perpendicular to the crack, but a conducting crack intensifies the field applied parallel to the crack.

alternating field, a crack perpendicular to the applied field grows stably, much like a fatigue crack in metals under cyclic stressing. The mechanism of this phenomenon remains unclear and will not be discussed further in this paper.

The signs of driving force have been established in previous works by explicit solutions of field equations (McMeeking, 1990; Pak, 1990; Suo *et al.*, 1992). In this section, the original idea of Griffith (1921) is extended in two ways, first to include electrical loading for cracks and thereby reconciling the signs of the crack driving force from a uniform viewpoint, and then to study conductive tubular channels.

2.1. *Crack growth*

The basic notation and field equations are listed in Appendix A. Subjected to a combined electric and stress field, of magnitude below a certain level, the dielectric is reversible but possibly nonlinear. The material is specified by an energy density function $\psi(\gamma, \mathbf{D})$ in accordance with

$$\mathrm{d}\psi = \sigma_{ij}\,\mathrm{d}\gamma_{ji} + E_i\,\mathrm{d}D_i. \tag{2.1}$$

The energy is stored by reversible distortion of electron clouds, macroscopically reflected by polarization and strain. Next consider a crack extending in the material. As the front moves, the intense field near the front moves electrons and ions irreversibly in thin layers beneath the crack surfaces. The irreversible movements, e.g. dislocation and charge motions, cannot be described by the energy function ψ, and have to be characterized independently. The details of the irreversible mechanisms, to be studied in later sections, are unnecessary for the Griffith energy balance.

The applied work is partly stored in the sample by the reversible distortion, and partly spent to create the irreversible layers. Thus,

$$F\,\mathrm{d}\Delta + V\,\mathrm{d}Q = \mathrm{d}\Psi + \Gamma\,\mathrm{d}A. \tag{2.2}$$

Here F and V are applied force and voltage, Δ and Q are work-conjugate displacement and charge, Ψ is the energy stored in the sample by reversible distortion, A is the crack area, and Γ is the work to create a unit area of the two irreversible layers. Note that Γ includes both the dissipated heat and the trapped energy remaining in the irreversible layers.

The thickness of the irreversible layers is usually much smaller than the sample dimension; they are therefore treated as *boundary layers*. In computing Ψ, the crack front is taken to be a mathematical line and the crack faces mathematical planes, disregarding the irreversible layers. Consequently, the boundary value problem is well-posed by the energy density function ψ and the basic field equations in Appendix A. Once the field in the sample is solved, a volume integration of ψ gives Ψ. Observe that Ψ depends on Δ, Q, A, and with increments varies as

$$\mathrm{d}\Psi = F\,\mathrm{d}\Delta + V\,\mathrm{d}Q - \mathscr{G}\,\mathrm{d}A. \tag{2.3}$$

When A remains fixed, (2.3) conserves energy. All other quantities being specified, (2.3) defines $\mathscr{G}$ as the driving force for crack area A. Note that $\mathscr{G}$ can be computed from the electroelasticity problem once Ψ is known. A combination of (2.2) and (2.3) shows that the crack cannot grow if $\mathscr{G} < \Gamma$.

Since $\mathcal{G}$ is defined to be independent of the irreversible mechanisms, its properties can be discussed on general grounds. Consider the sign of $\mathcal{G}$ for an experimental setup dominated by the electrical response. For a fixed crack size A, the V–Q curve looks like that in Fig. 2(a), either linear or nonlinear depending on the material; Ψ is the area under the curve. Now perform another experiment with an identical sample having slightly bigger crack area $A+\mathrm{d}A$. Figure 2(b) displays the two V–Q curves; the shaded area between the two curves is $\mathrm{d}\Psi$ associated with $\mathrm{d}A$. Equation (2.3) becomes

$$\mathrm{d}\Psi = -\mathcal{G}\,\mathrm{d}A, \quad Q \text{ held fixed.} \tag{2.4}$$

If the ceramic sample has larger permittivity than the medium inside the crack, the same voltage will induce less charge on the electrodes of the sample having the larger crack—that is, the V–Q curve for the sample having crack $A+\mathrm{d}A$ lies above the V–Q curve for the sample having crack A [Fig. 2(b)]. Consequently, $\mathrm{d}\Psi > 0$, and from (2.4) $\mathcal{G} < 0$. Conversely, for a ceramic sample having smaller permittivity than the medium inside the crack, $\mathrm{d}\Psi < 0$ and $\mathcal{G} > 0$. As special cases, $\mathcal{G} < 0$ for an insulating crack in a high permittivity ceramic, and $\mathcal{G} > 0$ for a conducting crack. (A conductor is regarded to have infinite permittivity.)

Two examples of $\mathcal{G}$ for conducting cracks follow. First consider a bilayer capacitor made of a linear dielectric with permittivity ε (Fig. 3). The electrode in the middle is a crack filled with an electrolyte solution. The layer thickness h is much smaller than the lateral dimensions, so that the electric field is confined within the area A, and the field distortion at the edge of the terminated electrode changes total energy insignificantly. Consequently, the solution for a parallel-plate capacitor applies:

$$Q = \varepsilon A V/h, \quad \Psi(Q, A) = VQ = hQ^2/\varepsilon A. \tag{2.5}$$

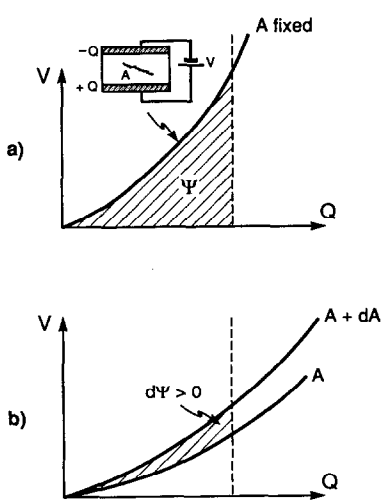

FIG. 2. (a) The reversible energy stored in the sample, Ψ, is the area under the V–Q curve. (b) $\mathrm{d}\Psi > 0$ when the ceramic has larger permittivity than the medium inside the crack.

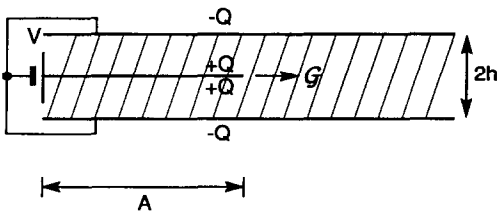

FIG. 3. An extending electrode in a bilayer capacitor.

Differentiating Ψ with respect to A gives

$$\mathcal{G} = \varepsilon V^2/h. \tag{2.6}$$

For example, a high permittivity device with $\varepsilon = 10^{-7}$ F m^{-1} and $h = 10^{-4}$ m, subjected to an applied field $V/h = 10^6$ V m^{-1}, has a driving force $\mathcal{G} = 10$ J m^{-2} on the terminated electrode.

Next consider the analogue of the Griffith crack, i.e. a conducting crack of size $2a$ in an infinite material subjected to an electric field E in the crack direction. The solution is (McMEEKING, 1990)

$$\mathcal{G} = \pi\varepsilon E^2 a/2. \tag{2.7}$$

This may be obtained by invoking the analogy between this problem and a crack under anti-plane shear stress, as summarized in Appendix B.

2.2. *Tubular channel*

Dielectric breakdown usually causes damage along a fine tubular channel, since little driving force exists sideways in the trail of a channel. The applied work is partly stored in the body by the reversible distortion, and partly spent to create the channel:

$$V\,\mathrm{d}Q = \mathrm{d}\Psi + \gamma\,\mathrm{d}L, \tag{2.8}$$

where L is the length of the channel, and γ the work to create a unit length of the channel. Only the electrical loading is considered here. The stored energy can be computed from the boundary value problems, and with increments varies as

$$\mathrm{d}\Psi = V\,\mathrm{d}Q - g\,\mathrm{d}L. \tag{2.9}$$

This equation defines the driving force g. A comparison of (2.8) and (2.9) shows that the channel cannot grow if $g < \gamma$.

Features specific to tubular channels are best illustrated by examples. Sketched in Fig. 4 is a slender dielectric cylinder of radius a, inserted with a needle-shaped electrode, wrapped by an electrode foil on the cylindrical surface but not the two bases, loaded by voltage V. A conductive channel, radius λ and length L, emanates from the needle tip. The field vanishes far ahead of the channel tip; behind the tip, the field is confined in the cross-sectional plane of the cylinder, pointing from the channel to the surface electrode. The electric potential at distance r from the center

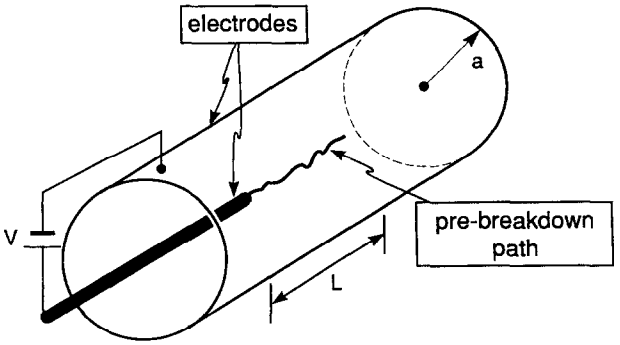

FIG. 4. An extending tubular pre-breakdown path.

of the channel is

$$\phi = -V \ln (r/\lambda)/\ln (a/\lambda). \tag{2.10}$$

The total charge induced on the channel is therefore

$$Q = 2\pi\varepsilon VL/\ln (a/\lambda). \tag{2.11}$$

The energy stored in the sample is $\Psi(Q, L) = VQ/2$. Differentiating Ψ with respect to L gives

$$\mathcal{G} = \pi\varepsilon V^2/\ln (a/\lambda). \tag{2.12}$$

The solution is valid so long as the channel length L is several times the cylinder radius a. This setup warrants a steady-state where $\mathcal{G}$ is invariant as L increases. Setups using slabs can also give rise to the steady-state; slabs with varying thickness can even make $\mathcal{G}$ decrease as the channel extends. Thus, by choosing the sample configuration, the breakdown path may grow slowly.

As a second example, consider a conductive prolate-spheroid, radius λ and length $2a$ ($a/\lambda \gg 1$), embedded in an infinite dielectric, subjected to an electric field E at infinity in the a-direction. Compared with the body without the spheroid, the energy stored in the body with the spheroid increases by (BEKER, 1982, p. 124)

$$\Delta\Psi = \frac{2\pi}{3}\varepsilon E^2 a^3/(\ln 2\alpha - 1), \tag{2.13}$$

where $\alpha = a/\lambda$ and the above is valid when $\alpha \gg 1$. Thus,

$$\mathcal{G} = \frac{\partial(\Delta\Psi)}{\partial(2a)} = \frac{\pi}{3}\varepsilon E^2 a^2 \frac{3\ln 2\alpha - 4}{(\ln 2\alpha - 1)^2}. \tag{2.14}$$

Note that $\mathcal{G}$ increases with a, suggesting unstable growth.

2.3. *Breakdown strength reduced by conducting defects*

First consider crack-like growth. The defect size $2a$ is assumed to be much smaller than the sample dimension. The dielectric breaks down when $\mathcal{G}$ in (2.7) reaches Γ.

Disregarding the numerical factor of order unity, one obtains the breakdown strength

$$E_B \approx (\Gamma/\varepsilon a)^{1/2}. \tag{2.15}$$

Note that E_B is inversely proportional to the square-root of the defect size.

Next, consider the needle-shaped conductive defect in an infinite material. The breakdown strength is obtained when g in (2.14) reaches γ. Thus,

$$E_B \approx (\gamma/\varepsilon)^{1/2}/a. \tag{2.16}$$

The numerical factor of unity is again ignored, together with the logarithmic dependence on a. The breakdown strength is inversely proportional to the defect size.

2.4. *On the channel radius*

Unlike a crack, a tubular channel cannot be idealized as a volumeless mathematical line in computing the stored energy. Nonetheless, only a rough value of the radius need be specified since it appears in the logarithmic function. A subtlety arises from this dependence on channel radius: the Irwin-type universal field does *not* exist at the tip of a tubular channel, for the near-tip field depends on the shape of the tip. As later discussion will demonstrate, this subtlety is more mathematical than physical. Retrospectively, K-field, HRR-field and the like, however prominent in correlating engineering quantities, are mathematical artifacts; they are sometimes convenient but never indispensable in uncovering physical processes. This statement may sound strange in a paper attempting to promote the ideas of fracture mechanics, but repeatedly suggests itself in recent investigations. For example, an understanding of metal–ceramic interface fracture resistance has emerged over the last few years, even though no acceptable nonlinear universal field has been found; see SUO and SHIH (1992) and references therein. Another example involves large-scale crack bridging, where adherence to crack tip field dogma has hindered progress (see BAO and SUO, 1992).

3. DIELECTRIC CRYSTALS

The Griffith energy balance requires little—nor does it uncover much—knowledge about the physical process of fracture/breakdown, but it does allow the resistance, Γ or γ, to be determined by testing a calibrated sample. In contrast to conventional breakdown strength, breakdown resistance is insensitive to the presence of defects. This semi-empirical approach is likely to be fruitful, at least to rank existing materials. Models presented in the following sections go one step further, to relate breakdown resistance to physical mechanisms.

3.1. *An estimate of theoretical strength*

Several estimates of breakdown strength exist in the literature (e.g. O'DWYER, 1973), but a particularly revealing one, i.e. the analogue of Frenkel's shear strength, does not seem to have been discussed. For simplicity, consider a nonpolar cubic

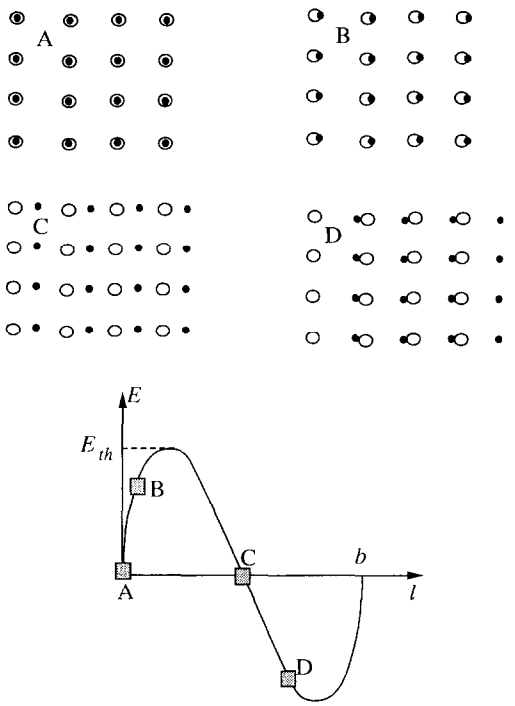

FIG. 5. Equilibrium states of a crystal subjected to an electric field.

crystal in Fig. 5; the solid dots represent the center of the mobile electron cloud, and the circles represent the ions. The crystal is perfect so the center of the electron cloud in every unit cell displaces by the *same* distance l when subjected to a field E. The E–l curve in Fig. 5 characterizes the *equilibrium states* of the crystal under the electric field, with states A, B, C and D marked. As l increases, the field needed to maintain the equilibrium increases, reaching the maximum—the theoretical strength E_{th}—at some $l < b/2$. At $l = b/2$, the electron cloud has the equal tendency to displace towards either direction, so that $E = 0$. When $l > b/2$, a field in the opposite direction must be applied to maintain the equilibrium. The E–l curve repeats itself periodically after $l = b$. Owing to the instabilities, this equilibrium curve may never be measured from a macroscopic sample, but may be realized in a localized region.

Take the equilibrium E–l curve to be sinusoidal in the spirit of Frenkel,

$$E = E_{\text{th}} \sin(2\pi l/b). \tag{3.1}$$

The curve maintains several essentials: (1) the maximum is the theoretical strength E_{th}, (2) the period is set by the lattice spacing b, and (3) the curve has a finite slope as $l/b \to 0$ to be fitted by permittivity. Let q be the charge of the mobile electron cloud for each unit cell, so that the polarization is ql/b^3. For small l/b, the polarization is linear with the applied field

$$ql/b^3 = (\varepsilon - \varepsilon_0)E, \tag{3.2}$$

where ε is the permittivity of the crystal and ε_0 the permittivity of a vacuum. Comparing (3.2) with (3.1) at the limit $l/b \to 0$, one obtains an estimate of the theoretical strength

$$E_{th} = \frac{q}{2\pi b^2(\varepsilon - \varepsilon_0)}. \tag{3.3}$$

Note that q/b^2 is the mobile charge per unit area in the plane normal to the applied field direction. With representative numbers $q = 1.6 \times 10^{-19}$ C, $b = 4 \times 10^{-10}$ m and $\varepsilon = 5\varepsilon_0 = 5 \times 8.85 \times 10^{-12}$ F m^{-1}, one obtains $E_{th} = 4.5 \times 10^9$ V m^{-1}. This value has the same order of magnitude as the strength of mica measured with small samples.

3.2. *Electron emission from the tip of a conducting channel*

In the above discussion, all the electrons are constrained to displace by the same amount. Now consider a conducting channel inside the crystal of diameter comparable to the lattice constant (Fig. 6). The electric field is intensified at the tip of the channel, so that the electrons near the tip displace more than those in the background. Inside the row directly ahead of the channel, the electrons displace according to the periodic law as in (3.1). Outside the row the material is taken to be linear dielectric. The flux of the polarization through the row is

$$\Omega = b^2 \times (ql/b^3) = ql/b. \tag{3.4}$$

Thus, the E–Ω relation is identical to the E–l relation except for the factor q/b. (The contribution by the linear permittivity should be excluded; this refinement is not included here). An electron emits from the channel tip when it is displaced to the unstable equilibrium state $l = b/2$, or $\Omega = q/2$. This corresponds to

$$\gamma = \int_0^{q/2} E(\Omega)\, d\Omega. \tag{3.5}$$

Using the sinusoidal curve in (3.1), one obtains $\gamma = E_{th}q/\pi$. With the same number used before, one finds that $\gamma \sim 10^{-10}$ N. This is the lower bound to the breakdown resistance, which may be substantially increased in two ways. First, the conducting

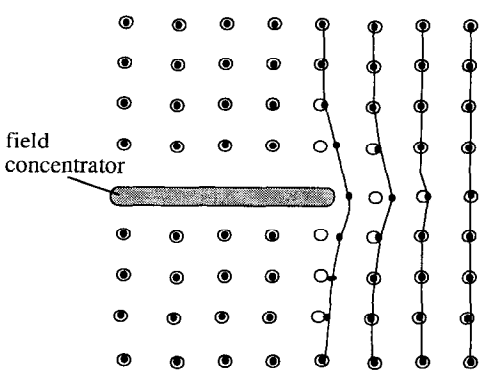

FIG. 6. Extra displacement of electrons ahead of an atomic-scale field concentrator.

channel may be composed of many rows of crystal cells. Second, energy in addition can be dissipated by background conduction.

The above model parallels Peierls model of dislocations; see Rice (1992) for a review on the latter. Several differences should be appreciated with this analogy. A dislocation affects atoms within a cylinder, but a trapped charge only affects atoms within a spot. Another difference lies in the mobility. When a pair of dislocations is created, the positive and negative dislocations have the same mobility, running in the opposite directions, leaving the crystal lattice otherwise undistorted—that is, dislocation can only pile up by other mechanisms, such as a grain boundary or a dislocation wall. When an electron–hole pair is created, the electron usually has higher mobility than the hole. This asymmetry might be ultimately responsible for charge clustering in a region elongated along the field direction, mediating breakdown.

3.3. *Role of dielectric loss*

When a constant field is suddenly applied to a dielectric, various polarization mechanisms take time to respond, so that the charges induced on the electrodes increase with time. This phenomenon defines a time-varying dielectric constant

$$\varepsilon(t) = \varepsilon_s \alpha(t/t_0), \tag{3.6}$$

where α is a monotonically increasing function, t_0 the relaxation time, and ε_s the static permittivity so that $\alpha(\infty) = 1$. The initial value, $\alpha_0 = \alpha(0)$ measures the extent of dielectric loss. A convolution integral gives the electric displacement induced by an arbitrary history of an applied field.

Dielectric loss affects breakdown in a way analogous to viscoelasticity affecting fracture. Consider a steady growing conduction channel in a lossy dielectric, driven by a constant g. The breakdown mechanism is specified by an E–Ω relation, the scales of which are set by Ω_0 and E_0, respectively. The tip moves if g exceeds the area under the E–Ω curves; the speed of the tip, v, increases if higher g is applied. Dimensional considerations dictate that

$$v = \frac{1}{t_0}\left(\frac{\Omega_0}{\varepsilon_s E_0}\right)^{1/2} \mathscr{F}\left(\frac{g}{\Omega_0 E_0}, \alpha_0\right). \tag{3.7}$$

The dimensionless function $\mathscr{F}$ also depends on the radius of the channel, and on the shape of α and E–Ω curves. Other parameters being fixed, the smaller the value of α_0, the lossier the dielectric, and therefore the smaller the velocity. Consequently, dielectric loss stabilizes the channel growth. The model may be analysed like the analogous models of fracture.

In the above, the heat generated by dielectric loss is assumed to dissipate by thermal conduction, so that temperature remains unchanged. This is a reasonable approximation for small velocity. Under high-frequency field, heat can be trapped at the tip, locally melting the material, reducing breakdown resistance, or causing thermal breakdown, fatigue and treeing.

3.4. *Role of background conduction*

Charges play a role just like dislocations: they carry conduction and deformation, respectively. Both relieve field concentration and dissipate energy, and thereby enhance breakdown/fracture resistance. Like dislocations, space charges may pre-exist in the material, or be injected from surfaces (in particular, from electrodes). Impurities that encourage high field conductivity are likely to increase breakdown resistance. The roles of plasticity of various forms have been the central theme of fracture mechanics, leading to concepts of tough ceramic materials; see EVANS (1990) and SUO and SHIH (1992) for reviews. To elucidate the subject, a particular charge relocation mechanism is analysed in the following section.

4. BREAKDOWN-RESISTANT LAMINATES

It is known empirically that a laminate has higher breakdown strength than a single layer of the same total thickness (BRADWELL, 1983). In the simplest form, the laminate can be made of the same material. Subjected to a field normal to the laminate, a breakdown channel in one layer does not readily enter the next layer; instead, the interface breaks down to relieve the field concentration in the next layer. The laminate can be substantially toughened when (1) the interfaces are weak so that a breakdown channel damages large areas of the interfaces, and (2) the strength in each layer varies with the position statistically so that the channels in adjacent layers do not align. Oil-impregnated paper laminates work by these principles.

The breakdown resistance is further amplified by a laminate alternating with two dielectrics with different breakdown electric displacements, say $D_{B1} > D_{B2}$, because the damage can spread over many weaker layers before the stronger layers start to break down to fail the laminate. To better control the interface, in-between the two dielectrics is coated by a third material, selected primarily for low breakdown strength E_I, aside from mundane requirements of adhesion and stability. Varistors used to protect electronic systems against over voltage, e.g. doped ZnO ceramics, have the desired characteristics, being insulators below certain fields, and conductors above. Subjected to a field normal to the laminate, the weaker layers break down first, turning on the interface conduction, alternately piling up space charge of different signs [Fig. 7(a)]. Charge pileup decreases field gradient, spreading the load over a larger volume of the material.

Each of the stronger layers has a thickness h, and the volume fraction of the stronger dielectric is f. For convenience, the inverse of permittivity, β, will be used as in $\mathbf{E} = \beta\mathbf{D}$. The effective dielectric property normal to the laminate is

$$\beta = f\beta_1 + (1-f)\beta_2. \tag{4.1}$$

Field distribution after the weaker layers break down is complicated; a few simplifications are to be made to gain insight into the matter. The model is a close analogue of that of fiber pullout in ceramic composites.

To be conservative in estimating the effect, strength within each layer is assumed to have no statistical variation so that all the channels align. Focus on one stronger

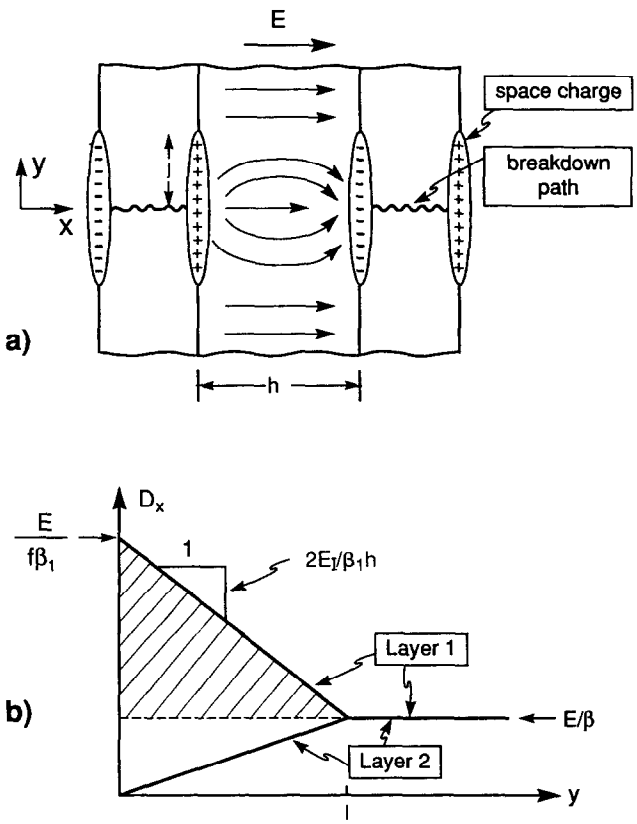

FIG. 7. (a) Field concentration is partially relieved in the stronger layer by interface damage. (b) Distribution of electric displacements.

layer between two adjacent weaker layers in Fig. 7(a), subjected to field E. The following calculates the electric displacement flux Ω owing to the damage. The interfaces are assumed to break down over a circular disk of radius l. The interface, or coating, is weak so that $l/h \gg 1$. Consequently, E_x in layer 1 is essentially independent of x. The damaged interfaces maintain field $E_y = \pm E_1$, giving rise to field lines in Fig. 7(a). Recall that the contour integral of the tangential component of the electric field is zero. A contour integral around an element $h \times dy$ yields

$$\frac{dE_x}{dy} + \frac{2E_1}{h} = 0. \tag{4.2}$$

This equation can also be derived from the standard field equation (B.6), in conjunction with the simplifying approximation that E_y varies linearly with x.

From (4.2), E_x varies linearly with y, with slope $-2E_1/h$. This is drawn in terms of electric displacement in Fig. 7(b); the variation in layer 2 is also included. Note that D_x is continuous across the undamaged interface beyond $y > l$, given by $D_x = E/\beta$

for both layers. At $y = 0$, layer 2 carries no load, and layer 1 carries all the load, so that $D_x = E/f\beta_1$. The breakdown radius is therefore

$$l = \frac{h}{2}\frac{(1-f)\beta_2}{f\beta}\frac{E}{E_1}. \tag{4.3}$$

The interface has much lower breakdown strength than the laminate, so that, indeed, $l \gg h$.

The damage-induced flux Ω is obtained by integrating $(D_{x1} - E/\beta)$ over the damage disk. Mathematically, this corresponds to the volume of the cone formed by revolving the shaded triangle around the D_x-axis in Fig. 7(b). Thus,

$$\Omega = \frac{\pi h^2}{12}\left[\frac{(1-f)\beta_2}{f\beta}\right]^3 \frac{E^3}{\beta_1 E_1^2}. \tag{4.4}$$

Equation (4.4) is readily inverted to give the $E(\Omega)$ curve. Denote Ω_0 as the flux at the failure field $E = fE_{B1}$. The breakdown resistance is therefore

$$\gamma = \int_0^{\Omega_0} E(\Omega)\,\mathrm{d}\Omega = \frac{\pi h^2}{16}\left[\frac{(1-f)\beta_2}{f\beta}\right]^3 \frac{(fE_{B1})^4}{\beta_1 E_1^2}. \tag{4.5}$$

Note that γ is large when the interface is weak. Using representative numbers $h = 10^{-4}$ m, $\varepsilon = 10^{-10}$ F m^{-1}, $E_{B1} = 10^8$ V m^{-1}, $E_1 = 10^5$ V m^{-1}, one finds that $\gamma \sim 10^3$ N. Note the substantial difference between the laminates and the perfect crystal.

The exact architecture of the composite is unimportant. Aligned platelets in a matrix would achieve the same effect, so long as the volume fraction of the platelets is high enough to prevent percolation, and each platelet has radius larger than l in (4.3), where E is replaced by an equivalent breakdown strength. High breakdown strength is derived from the high strength of the individual reinforcement; high breakdown toughness is achieved by large-scale charge relocation.

5. Cracks in Ferroelectrics Driven by Electric Fields

Cracks can grow in ferroelectric ceramics driven by electric field induced strain (Winzer *et al.*, 1989; Cao and Evans, 1993). To focus ideas, attention is restricted to unpoled ferroelectric ceramics, where domains are not aligned, and remain unswitched when subjected to a low electric field. As such, the materials are macroscopically indistinguishable from linear dielectrics. A pre-cut crack contains a conductive species, e.g. NaCl solution, mimicking environmental effects or internal discharge. The macroscopic field is summarized below, followed by a discussion of a cracking process.

5.1. *Field around the front of a conducting sheet*

Figure 8 illustrates a conducting crack of length a in a linear capacitor of thickness h, subjected to voltage V. Appendix B summarizes the well-known analogy between a conducting crack and a mode III elastic crack. This analogy, including boundary

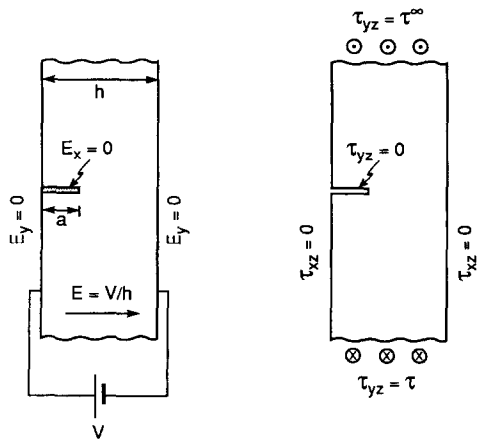

FIG. 8. A conducting sheet is mathematically equivalent to a mode III elastic crack.

conditions, is illustrated in Fig. 8. Let (r, θ) be the polar coordinate centered at the crack tip with crack faces lying on $\theta = \pm\pi$. The crack tip field found in electrodynamics textbooks is written

$$[E_x, E_y] = K_E(2\pi r)^{-1/2}[\cos(\theta/2), \sin(\theta/2)]. \tag{5.1}$$

The intensity factor $K_E > 0$ corresponds to the tip accumulating positive charges. Note that the magnitude of the field is independent of θ. The field ahead of the crack tip is directed towards the running direction of the crack, decaying with r as

$$E = K_E(2\pi r)^{-1/2}. \tag{5.2}$$

The charge accumulated on the crack plane, in a rectangular area of unit length along the front, from the tip to a distance r behind the tip, is

$$\delta = 4\varepsilon K_E(r/2\pi)^{1/2}. \tag{5.3}$$

This quantity has the unit of charge per unit length.

Consider two bodies with slightly different crack lengths, a and $a+l$, where $l \ll a$, each loaded with K_E. Following the elasticity analogue of IRWIN (1957), the difference in the energy stored in the two bodies equals the virtual work of the field E_x ahead of crack a, done through the flux δ behind crack $a+l$. From (3.2) and (3.3) it follows that

$$\mathcal{G} = \frac{1}{2l}\int_0^l \left[\frac{K_E}{(2\pi x)^{1/2}}\right]\left[4\varepsilon K_E\left(\frac{l-x}{2\pi}\right)^{1/2}\right]dx, \tag{5.4}$$

so that

$$\mathcal{G} = \tfrac{1}{2}\varepsilon K_E^2. \tag{5.5}$$

This equation establishes that $\mathcal{G}$ and K_E are equivalent loading parameters.

Following Irwin's interpretation, we emphasize that (5.1) is valid only in the region

where r is larger than some nonlinear zone size, but smaller than the sample dimension. The intensity factor K_E serves as a messenger between the external loading and the near-tip process. For example, K_E for the crack in Fig. 8 is

$$K_E = E[2h \tan(\pi a/2h)]^{1/2}. \tag{5.6}$$

Relations connecting K_E and applied loads for other geometries can also be extracted from fracture mechanics handbooks.

5.2. *A conducting crack extension process*

Relations between K_E and near-tip processes depend on mechanisms. Owing to limited experiments, mechanism-based theories are too speculative to warrant detailed analysis at this point. A likely mechanism, by which a conducting sheet extends under electric fields, is proposed here with a heuristic analysis.

The intensified electric field at the front of a conducting sheet rotates dipoles [Fig. 9(a)]. From (5.1), the magnitude of the field decays with r according to $E = K_E(2\pi r)^{-1/2}$. The radius of the switching zone, R, is estimated by letting $E = E_c$, E_c being the coercive field. Thus

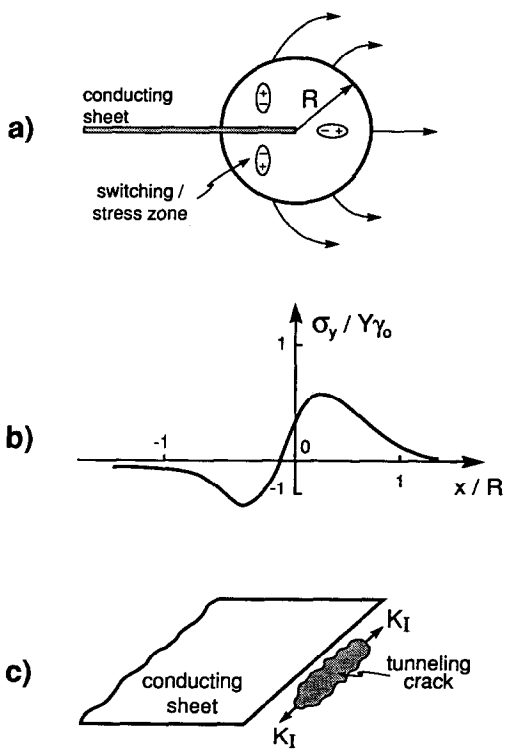

FIG. 9. (a) The intensified electric field at the front of a conducting sheet induces ferroelectric switching. (b) The anticipated stress distribution. (c) The tensile stress ahead of the conducting sheet drives a microcrack to tunnel parallel to the front of the sheet.

$$R = \frac{1}{2\pi}(K_E/E_c)^2. \tag{5.7}$$

For a given material, R increases with applied load K_E.

Associated with the dipole rotation is a shear strain, γ_0, with representative value for actuator ceramics $\gamma_0 \sim 10^{-3}$. A stress field is induced by the strain owing to the constraint of the unswitched material in the background. Features relevant to cracking can be inferred as follows. First, the stress field is localized within a region scaled by R. Second, the magnitude of the stress scales with $Y\gamma_0$, Y being Young's modulus. Third, the normal stress component, σ_{yy}, is tensile ahead of the sheet front but compressive behind the front, as judged from the dipole orientations in these regions. These observations are sketched in Fig. 9(b), and written as

$$\sigma_{yy} = Y\gamma_0 F(x/R). \tag{5.8}$$

The dimensionless function F is of order unity and takes the shape of Fig. 9(b).

The localized, tensile stress can drive a pre-existing microcrack in the ceramic to *tunnel* parallel to the front of the conducting sheet [Fig. 9(c)]. The situation is similar to micro-tunnels in composites caused by thermal mismatch strains (HO and SUO, 1992). The tunnel grows when

$$K_{Ic} \sim Y\gamma_0\sqrt{R}, \tag{5.9}$$

where K_{Ic} is the fracture toughness of the ceramic.

Combining (5.7) and (5.9) gives an estimate of the critical K_E to form a tunnel

$$K_{Ec} \sim \sqrt{2\pi}E_c K_{Ic}/Y\gamma_0. \tag{5.10}$$

The process repeats itself at the new front once the conducting species diffuse into the tunnel. Taking $E_c = 10^6$ V m^{-1}, $K_{Ic} = 10^6$ Pa m$^{1/2}$, and $Y\gamma_0 = 10^8$ Pa, one finds from (5.10) that $K_{Ec} \sim 10^4$ V m$^{1/2}$. For a ferroelectric with $\varepsilon \sim 10^{-8}$ F m^{-1}, this corresponds to a load $\mathscr{G} \sim 1$ J m^{-2}, a magnitude readily achievable in actuators. Observe that the entire process does *not* require the conducting sheet as a whole to open; the sheet is therefore likely to be a network of microcracks. Also observe that the growth of the conducting sheet is diffusion-limited, and therefore stable. One may predict growth rate once a diffusion mechanism is specified.

6. PIEZOELECTRICS

Piezoelectric ceramics have an additional complication: the electrical and mechanical responses couple even at macroscopic scale. The ceramics are assumed to be linearly piezoelectric, ferroelectric switching being localized at the crack tip. Crack growth mechanisms are expected to be similar to unpoled ferroelectrics. Impermeable cracks in piezoelectrics have been analysed by PAK (1990), SOSA and PAK (1990), SHINDO *et al.* (1990), and SUO *et al.* (1992), but no such analysis is available for conducting cracks. The analysis of conducting cracks is greatly simplified by a formulation in terms of the charge potential, as described in Appendix C. The main results are outlined below.

6.1. *General anisotropy*

First consider the eigenvalue problem with a half-plane crack lying in an infinite body of a piezoelectric. The stress and electric field vanish far away from the crack front; the crack is traction-free and conductive, i.e.

$$\sigma_{2j} = E_1 = 0, \quad \text{on } x_1 < 0, x_2 = x_3 = 0. \tag{6.1}$$

These boundary conditions can be imposed on $\mathbf{f}(z)$ by using (C.9). The solution is

$$B\mathbf{f}(z) = (z/2\pi)^{1/2}\mathbf{k}, \tag{6.2}$$

where $\mathbf{k}$ is a real-valued column consisting of four intensity factors

$$\mathbf{k} = \{K_{II}, K_I, K_{III}, K_E\}. \tag{6.3}$$

The field quantities can be derived from (C.8–10), with z_α substituted into each of f_α. In particular, one can confirm that at a distance r ahead of the crack tip

$$\{\sigma_{2j}, E_1\} = (2\pi r)^{-1/2}\mathbf{k}, \tag{6.4}$$

and that at a distance r *behind* the crack tip

$$\{\delta_j, \delta\} = (2r/\pi)^{1/2}H\mathbf{k}, \tag{6.5}$$

where δ_j is the displacement jump between the crack faces, and δ is the charge accumulated in the interval $-r < x < 0$. In general, H contains off-diagonal elements, so that K_E induces crack opening, and K_I induces charge. The crack driving force is related to the intensity factors by

$$\mathscr{G} = \tfrac{1}{4}\mathbf{k}^T H\mathbf{k}. \tag{6.6}$$

Since H is positive-definite, $\mathscr{G} > 0$ for any singularity mode.

Next consider a crack of length $2a$, on the x_1-axis, in an infinite piezoelectric body, subjected to a remote load $\mathbf{T} = \{\sigma_{2j}^\infty, E_1^\infty\}$. Suo *et al.* (1992) showed that, for a class of problems, solutions in terms of $B\mathbf{f}(z)$ are identical to that of a mode III crack in an isotropic elastic body. Thus,

$$B\mathbf{f}(z) = \tfrac{1}{2}\mathbf{T}(z^2 - a^2)^{1/2}. \tag{6.7}$$

Comparing (6.7) with (6.2) at the crack tip gives

$$K_I = \sqrt{\pi a}\sigma_{22}^\infty, \quad K_E = \sqrt{\pi a}E_1^\infty. \tag{6.8}$$

The results are identical to those for isotropic dielectrics, a coincidence specific to the geometry. Thus, within the linear piezoelectricity formulation, the electric field does not induce any tensile stress directly ahead of a small crack. This observation indicates that mechanism-based models such as discussed in Section 5 are required even for a qualitative understanding of crack growth in piezoelectrics under electrical loading.

6.2. *Poled ferroelectric ceramics*

A poled ferroelectric ceramic is linearly piezoelectric up to a certain load level, and transversely isotropic about the poling axis, labeled as axis 3. The constitutive law

and other background information are contained in JAFFE *et al.* (1971). Three principal crack orientations will be treated as follows.

First consider the crack with its front coincident with the x_3-axis. The in-plane elastic deformation is decoupled from the electric field and anti-plane deformation. The former will be eliminated from the discussion. Following the notation in Appendix C, the relevant constitutive law is

$$\begin{bmatrix} \sigma_{13} \\ \sigma_{23} \\ E_1 \\ E_2 \end{bmatrix} = \begin{bmatrix} c_{44} & 0 & h_{15} & 0 \\ 0 & c_{44} & 0 & h_{15} \\ h_{15} & 0 & \beta_{11} & 0 \\ 0 & h_{15} & 0 & \beta_{11} \end{bmatrix} \begin{bmatrix} \gamma_{13} \\ \gamma_{23} \\ D_1 \\ D_2 \end{bmatrix}. \tag{6.9}$$

The crack tip field can be specialized from Section 6.1. In particular, E_1 and σ_{23} are square root singular, K_{E} and K_{III} being defined according to (6.4). The driving force relates to the intensity factors by

$$\mathscr{G} = \frac{\beta_{11}K_{\mathrm{III}}^2 + c_{44}K_{\mathrm{E}}^2}{2(c_{44}\beta_{11} - h_{15}^2)}. \tag{6.10}$$

As pointed out earlier, both intensities give positive driving force.

Next consider a crack running in the x_3-direction. The anti-plane deformation is decoupled from the in-plane deformation and electric field, and therefore eliminated from the following. The driving force is related to the intensity factors by

$$\mathscr{G} = \tfrac{1}{2}s_1K_{\mathrm{I}}^2 + \frac{\varepsilon}{2}K_{\mathrm{E}}^2 + \mathrm{d}K_{\mathrm{I}}K_{\mathrm{E}} + \tfrac{1}{2}s_3K_{\mathrm{II}}^2. \tag{6.11}$$

Some coefficients vanish because of symmetry; for example, a K_{E} field does not induce a sliding displacement between the crack faces, so that the term $K_{\mathrm{E}}K_{\mathrm{II}}$ drops out. The non-zero coefficients can be computed numerically (SUO *et al.*, 1992).

Finally, for a crack lying in the plane normal to x_3, the driving force takes the form

$$\mathscr{G} = \tfrac{1}{2}s_1K_{\mathrm{II}}^2 + \frac{\varepsilon}{2}K_{\mathrm{E}}^2 + \mathrm{d}K_{\mathrm{II}}K_{\mathrm{E}} + \tfrac{1}{2}s_3K_{\mathrm{I}}^2. \tag{6.12}$$

Since the matrix H behaves like a tensor with an in-plane rotation (SUO *et al.*, 1992), the coefficients in (6.11) and (6.12) take corresponding values as indicated.

7. CONCLUDING REMARKS

A perspective on breakdown-resistant composites emerges from the discussion, although many details might be refined or even altered as the experience accumulates. Tubular growth of a breakdown path can be studied by Griffith energy balance. A breakdown process consists of two basic elements: (1) space charge relocation that forms a conductive channel and, (2) dissipation by dielectric loss and electrical conductivity within a localized region. The former leads to an intensified electric field that activates the background dissipation; the latter shields the channel tip from the applied

field and, under some conditions, locally heats the material to melting. Breakdown resistance can be substantially enhanced by large-scale charge relocation, as in layered materials with varistor coatings. Crack-like growth under electrical loading has been observed experimentally in many ferroelectric actuator materials. Unlike electronic breakdown, these cracks are expected to be driven by localized tensile stresses. To make further progress, it is imperative to design and conduct critical experiments on dielectric laminates and ferroelectric ceramics.

Acknowledgements

The author is grateful to D. R. Clarke for suggesting the investigation on tubular channels. The work is supported by the National Science Foundation through grant MSS-9258115, and by the Office of Naval Research through contract N00014-93-1-0110.

References

Bao, G. and Suo, Z. (1992) Remarks on crack-bridging concepts. *Appl. Mech. Rev.* **45,** 355–366.

Becker, R. (1982) *Electromagnetic Fields and Interaction.* Dover Publications, New York.

Bradwell, A. (1983) *Electrical Insulation.* Peter Peregrinus, London.

Cao, H. C. and Evans, A. G. (1993) Electric field-induced fatigue crack extension in ferroelectric ceramics. Submitted for publication.

Devine, R. A. B. (1988) *The Physics and Technology of Amorphous* SiO_2. Plenum Press, New York.

Evans, A. G. (1990) Perspective on the development of high-toughness ceramics. *J. Am. Ceram. Soc.* **73,** 187–206.

Freiman, S. W. and Pohanka, R. C. (1989) Review of mechanically related failures of ceramic capacitors and capacitor materials. *J. Am. Ceram. Soc.* **72,** 2258–2263.

Griffith, A. A. (1921) The phenomena of rupture and flow in solids. *Phil. Trans. R. Soc. Lond.* **A221,** 163–197.

Ho, S. and Suo, Z. (1992) Microcracks tunneling in brittle matrix composites driven by thermal expansion mismatch. *Acta Metall. Mater.* **40,** 1685–1690.

Irwin, G. R. (1957) Analysis of stresses and strains near the end of a crack traversing a plate. *J. Appl. Mech.* **24,** 361–364.

Jaffe, B., Cook, W. R., Jr and Jaffe, H. (1971) *Piezoelectric Ceramics.* Academic Press, London.

McMeeking, R. M. (1990) A J-integral for the analysis of electrically induced mechanical stress at cracks in elastic dielectrics. *Int. J. Engng Sci.* **28,** 605–613.

O'Dwyer, J. J. (1973) *The Theory of Electrical Conduction and Breakdown in Solid Dielectrics.* Clarendon Press, Oxford.

Pak, Y. E. (1990) Crack extension force in a piezoelectric material. *J. Appl. Mech.* **57,** 647–653.

Rice, J. R. (1992) Dislocation nucleation from a crack tip: an analysis based on Peierls concept. *J. Mech. Phys. Solids* **40,** 239–271.

Shindo, Y., Ozawa, E. and Nowacki, J. P. (1990) Singular stress and electric fields of a cracked piezoelectric strip. *Appl. Electromagnetics Mater.* **1,** 77–87.

Sosa, H. A. and Pak, Y. E. (1990) Three-dimensional eigenfunction analysis of a crack in a piezoelectric material. *Int. J. Solids Struct.* **26,** 1–15.

Suo, Z. (1991) Mechanics concepts for failure in ferroelectric ceramics. *Smart Structures and Materials* (ed. A. V. Srinivasan) pp. 1–6. ASME, New York.

Suo, Z., Kuo, C.-M., Barnett, D. M. and Willis, J. R. (1992) Fracture mechanics for piezoelectric ceramics. *J. Mech. Phys. Solids* **40,** 739–765.

SUO, Z. and SHIH, C. F. (1992) Models for metal/ceramic interface fracture. *Metal–Matrix Composites* (eds S. SURESH, A. MORTENSEN and A. NEEDLEMAN). Butterworth-Heinemann, Stoneham, MA.

WHITEHEAD, S. (1953) *Dielectric Breakdown of Solids*. Clarendon Press, Oxford.

WINZER, S. R., SHANKAR, N. and RITTER, A. P. (1989) Designing cofired multilayer electrostrictive actuators for reliability. *J. Am. Ceram. Soc.* **72,** 2246–2257.

APPENDIX A. CONTINUUM EQUATIONS

Subject a solid dielectric to a field of displacement $\mathbf{u}$ and electric potential ϕ. Small deformation is of concern for ceramics, so that the strain γ and the electric field $\mathbf{E}$ are derived from gradients

$$\gamma_{ij} = \tfrac{1}{2}(u_{i,j} + u_{j,i}), \quad E_i = -\phi_{,i}. \tag{A.1}$$

Stress tensor σ and electric displacement vector $\mathbf{D}$ were historically introduced on the basis of different physical principles. Yet they can be defined, from the same viewpoint, as work-conjugates to γ and $\mathbf{E}$, respectively. Consider a composite of conductors and dielectrics, with $\mathbf{t}$ the force and ω the charge, per unit area, externally supplied on the interfaces. The body force and space charge are taken to be negligible. The principle of virtual work is postulated:

$$\int (\sigma_{ij}\delta\gamma_{ji} + E_i\delta D_i)\,\mathrm{d}v = \int (t_i\delta u_i + \phi\delta\omega)\,\mathrm{d}s. \tag{A.2}$$

That is, for any virtual variation, the energy variation in the body equals the work applied at the interfaces.

Equations (A.1) and (A.2) define σ and $\mathbf{D}$. In particular, they imply, as can be verified by using the divergence theorem, that σ and $\mathbf{D}$ are divergence free:

$$\sigma_{ij,j} = 0, \quad D_{i,i} = 0, \tag{A.3}$$

and that across an interface, σ and $\mathbf{D}$ jump by

$$n_i[\sigma_{ij}^{+} - \sigma_{ij}^{-}] = t_j, \quad n_i[D_i^{+} - D_i^{-}] = -\omega, \tag{A.4}$$

where $\mathbf{n}$ is the unit normal to the interface pointing from the medium labeled as $+$.

APPENDIX B. 2D FIELD IN ISOTROPIC DIELECTRICS

Consider a two-dimensional field independent of x_3. When the sample is absent of space charge, $\mathbf{D}$ is divergence-free, so that a function $\xi(x_1, x_2)$ exists, giving

$$D_1 = \partial\xi/\partial x_2, \quad D_2 = -\partial\xi/\partial x_1. \tag{B.1}$$

The physical significance of ξ is interpreted by considering a curve s dividing the plane into regions $+$ and $-$. Let the normal vector $\mathbf{n}$ point from $+$ side; region $+$ is on the left of an observer traveling in the positive direction of the curve, so that

$$n_1 = \mathrm{d}y/\mathrm{d}s, \quad n_2 = -\mathrm{d}x/\mathrm{d}s. \tag{B.2}$$

The normal component of $\mathbf{D}$ is therefore

$$D_i n_i = \mathrm{d}\xi/\mathrm{d}s. \tag{B.3}$$

Consequently, ξ is the total flux of electric displacement normal to curve s. When curve s represents a discontinuity such as a conducting sheet or a damaged interface between two dielectrics, charge density ω accumulates on the curve. Define the discontinuity in the flux across s:

$$\delta = \xi^+ - \xi^-. \tag{B.4}$$

Combining (A.4) and (B.3) shows that

$$\mathrm{d}\delta = -\omega\,\mathrm{d}s. \tag{B.5}$$

Thus, the jump in ξ across the curve equals the charge accumulated on the entire curve. The function $\xi(x_1, x_2)$ is therefore called charge potential.

It follows from (A.1) that

$$\partial E_1/\partial x_2 - \partial E_2/\partial x_1 = 0. \tag{B.6}$$

For a linearly isotropic dielectric with permittivity ε, the field is related to electric displacement by

$$E_1 = \frac{1}{\varepsilon} D_1, \quad E_2 = \frac{1}{\varepsilon} D_2. \tag{B.7}$$

Observe that the mathematical equations for the dielectric problem is identical to that of an anti-plane deformation problem, with correspondence

$$\xi \to u_3, \quad -E_2 \to \sigma_{13}, \quad E_1 \to \sigma_{23}, \quad 1/\varepsilon \to \mu. \tag{B.8}$$

The general solution is given by an analytic function f of a complex variable z:

$$\xi = \varepsilon\,\mathrm{Im}\,[f(z)], \tag{B.9}$$

$$E_1 - \mathrm{i}E_2 = f'(z). \tag{B.10}$$

The function f is determined by boundary conditions.

Appendix C. A Complex Variable Representation of Piezoelectric Fields Using Charge Potential

A generally anisotropic, linearly piezoelectric material is characterized by an energy density function

$$\psi(\gamma, \mathbf{D}) = \tfrac{1}{2} C_{ijrs}\gamma_{ji}\gamma_{rs} + \tfrac{1}{2}\beta_{is}D_iD_s + h_{irs}D_i\gamma_{rs}, \tag{C.1}$$

so that the constitutive relations are

$$\sigma_{ij} = C_{ijrs}\gamma_{rs} + h_{sji}D_s, \quad E_i = \beta_{is}D_s + h_{irs}\gamma_{rs}. \tag{C.2}$$

Here C, β and h characterize elastic, dielectric and piezoelectric responses.

Equations (B.1–6) are still valid for piezoelectrics. To better organize notation, denote

$$\hat{D}_1 = -D_2, \quad \hat{D}_2 = +D_1,$$
$$\hat{E}_1 = -E_2, \quad \hat{E}_2 = +E_1. \tag{C.3}$$

Thus the governing equations become

$$\sigma_{ij,i} = 0, \quad \hat{E}_{i,i} = 0, \tag{C.4}$$

$$\gamma_{ij} = \tfrac{1}{2}(u_{i,j} + u_{j,i}), \quad \hat{D}_i = \xi_{,i}, \tag{C.5}$$

$$\sigma_{ij} = C_{ijrs}\gamma_{rs} + \hat{h}_{sji}\hat{D}_s, \quad \hat{E}_i = \hat{\beta}_{is}\hat{D}_s + \hat{h}_{irs}\gamma_{rs}, \tag{C.6}$$

where $\hat{h}$ and $\hat{\beta}$ are modified from (C.2). Observe that equations (C.4–5) have the same mathematical form as those in Suo *et al.* (1992) in terms of ϕ, with correspondence

$$\xi \to \phi, \quad \hat{D}_i \to E_i, \quad \hat{E}_i \to D_i. \tag{C.7}$$

The following results, as well as those in Section 6.1, are extracted from the earlier paper following the correspondence.

Let p_1, p_2, p_3 and p_4 be the characteristic roots with positive imaginary part, $\mathbf{a}_\alpha$ and $\mathbf{b}_\alpha$ be

the associated characteristic columns, and $z_\alpha = x + p_\alpha y$. They should be determined by an eigenvalue problem associated with (C.4–7). The characteristic roots should be identical to those in SUO *et al.* (1992), but the characteristic columns are different. The solution is a linear combination of four arbitrary functions:

$$\{u_i, \xi\} = 2\,\mathrm{Re}\sum_{\alpha=1}^{4} \mathbf{a}_\alpha f_\alpha(z_\alpha), \tag{C.8}$$

$$\{\sigma_{2j}, \hat{E}_2\} = 2\,\mathrm{Re}\sum_{\alpha=1}^{4} \mathbf{b}_\alpha f'_\alpha(z_\alpha), \tag{C.9}$$

$$\{\sigma_{1j}, \hat{E}_1\} = -2\,\mathrm{Re}\sum_{\alpha=1}^{4} \mathbf{b}_\alpha p_\alpha f'_\alpha(z_\alpha), \tag{C.10}$$

where Re stands for the real part, and f' for differentiation; f_1, f_2, f_3 and f_4 need only satisfy boundary conditions.

Define 4×4 matrices

$$A = [\mathbf{a}_1, \quad \mathbf{a}_2, \quad \mathbf{a}_3, \quad \mathbf{a}_4], \quad B = [\mathbf{b}_1, \quad \mathbf{b}_2, \quad \mathbf{b}_3, \quad \mathbf{b}_4], \tag{C.11}$$

and

$$Y = \mathrm{i}AB^{-1}, \tag{C.12}$$

where $\mathrm{i} = \sqrt{-1}$. Because ψ is positive-definite, Y is a positive-definite Hermitian matrix. By contrast, a similar matrix introduced in SUO *et al.* (1992) based on displacements and electric potential is indefinite. Also define

$$H = 2\,\mathrm{Re}\,Y. \tag{C.13}$$

H is real, symmetric and positive-definite.

The general solution involves four analytic functions, each depending on its own variable. Define a column of a *single variable*

$$\mathbf{f}(z) = \{f_1(z), f_2(z), f_3(z), f_4(z)\}^{\mathrm{T}}, \quad z = x + \zeta y, \quad \mathrm{Im}\,(\zeta) > 0. \tag{C.14}$$

To compute the field quantities from (C.8–10), one must substitute z_1, z_2, z_3 or z_4 for each component function.